JES Focus Issue of Selected Papers from IMLB 2018

Li^+ Insertion/Extraction Properties for $TiNb_2O_7$ Single Particle Characterized by a Particle-Current Collector Integrated Microelectrode

Ryoji Inada,[1,z] Rei Kumasaka,[1] Shuto Inabe,[1] Tomohiro Tojo,[2] and Yoji Sakurai[1,*]

[1]*Department of Electrical and Electronic Information Engineering, Toyohashi University of Technology, Tempaku-cho, Toyohashi, Aichi 441-8580, Japan*
[2]*Department of Electrical and Electronic Engineering, Shizuoka Institute of Science and Technology, Fukuroi, Shizuoka 437-8555, Japan*

In this study, we evaluate the electrochemical properties of $TiNb_2O_7$ (TNO) single particle using a particle-current collector integrated microelectrode, in which TNO single particle with the size of approximately 10 μm was bonded on the tip of a tungsten microelectrode by platinum deposition using a focused ion beam process unit (FIB). Cyclic voltammogram of TNO single particle showed the reversible redox peaks at around 1.6−1.7 V vs. Li/Li^+. Anodic peak current is higher than cathodic one at a fixed scan rate, indicating faster reaction during Li^+ extraction (i.e. discharge) than Li^+ insertion (i.e. charge) of TNO particle. This tendency was also confirmed in C-rate dependence of charge and discharge capacities. From the results for galvanostatic intermittent titration testing (GITT), we confirmed that at the equilibrium potential vs. Li/Li^+ below 1.5 V, apparent chemical diffusion coefficient of Li^+ in TNO at Li^+ extraction process is much larger than at Li^+ insertion process. Furthermore, the capacity retention of TNO single particle tested at current of 10C after 2000 cycles was above 99%, indicating excellent intrinsic stability of TNO single particle for Li^+ insertion and extraction reaction.

 [DOI: 10.1149/2.0241903jes]

Manuscript submitted October 29, 2018; revised manuscript received November 20, 2018. Published December 6, 2018. *This paper is part of the JES Focus Issue of Selected Papers from IMLB 2018.*

Lithium-ion batteries (LiB) have been used as power sources for various electronic devices, such as mobile phones and notebook computers. Graphite has been commonly used as an anode material for present LiB because of its low cost, acceptable storage capacity (= 372 mAh g^{-1}) and stable cycling performance. However, the passivating solid electrolyte interphase (SEI) formed on graphite electrode in the initial charging process by the decomposition of organic liquid electrolyte, which consumes some amount of lithium irreversibly. In addition, the low Li^+ storage potential of graphite raises safety issues: when charged at high current rate or overcharged, there is possible lithium plating or formation of lithium dendrites and the short circuit of the battery to fire the flammable electrolyte. Safety concern has become the serious issue for large scale applications of LiB, such as hybrid electric vehicles and energy storage system.[1–3] To overcome this problem, titanium-based oxides have attracted wide attention because of relatively high redox potential between 1.0 and 2.0 V vs. Li/Li^+, which eliminates the possibility of lithium plating during the charging process. Particularly, the zero-strain $Li_4Ti_5O_{12}$ (LTO) with cubic spinel structure was widely studied as a highly safe anode material for LiB due to its excellent cycle stability and high rate capability.[4–12] However, theoretical Li^+ storage capacity of LTO is limited to 175 mAh g^{-1}. Development of anode materials with similar properties but with high Li^+ storage capacity is strongly required for large scale applications.

Mixed titanium-niobium (Ti-Nb) oxides with the redox potentials from 1.0 to 2.0 V vs. Li/Li^+ have been also considered as interesting candidates for an anode material of LiB with high safety,[13–32] because it is possible to realize multi-electron transfer by redox couples of Ti^{4+}/Ti^{3+}, Nb^{5+}/Nb^{4+} and Nb^{4+}/Nb^{3+}, resulting into high Li^+ storage capacity. Moreover, these oxides are nontoxic and more importantly, their redox potential should avoid possible lithium plating. To date, the electrochemical properties for mixed Ti-Nb oxides such as $TiNb_2O_7$,[13–26] $Ti_2Nb_{10}O_{29}$[13,26–30] and $TiNb_{24}O_{62}$[13,31,32] are reported. They have the monoclinic "shear ReO_3 structure" with the space group of *C*2/*m*, consisting of MO_6 (M = Ti, Nb) octahedra sharing edges and corners.[12,13,25,30] Gravimetric theoretical capacity for these oxides is 390−400 mAh g^{-1} derived from the redox couples of Ti^{4+}/Ti^{3+}, Nb^{5+}/Nb^{4+} and Nb^{4+}/Nb^{3+} and at the potential above 1.0 V vs. Li/Li^+, they shows the reversible capacity of 250−300 mAh g^{-1}. Due to the true density (= 4.3−4.4 g cm^{-3}), their volumetric theoretical capacity attains to approximately 1700 mAh cm^{-3}, which is twice that of graphite (= 837 mAh cm^{-3}).

It has been reported that mixed Ti-Nb oxides show larger volume change (8−10%) than LTO (< 0.2%) during charge (Li^+ insertion) and discharge (Li^+ extraction) reactions.[19,23] In general, large volume change for electrode active materials during charge and discharge reactions causes the mechanical damage to the active material itself and/or degradation in the electrical conduction path in composite electrode composed of an active material, a carbon additive and an organic polymer binder, resulting into lower cycling stability. From a practical point of view, both controlling the size and morphology of active material particle and optimizing the composition of composite electrode are important to improve the cycling stability for composite electrode. Actually, introduction of nanostructure and controlling the particle morphology for mixed Ti-Nb oxide play an important role to improve the electrochemical performance in composite electrodes.[17–19,23,24,28–32] On the other hand, electrochemical reaction for a composite electrode may contain the side reaction for a carbon additive and a binder, so that the intrinsic electrochemical performance in active material itself would not be evaluated precisely from the experimental data for composite electrodes

The single particle measurement of active materials has been proposed by using a needle microelectrode, in which the tip is attached to a single particle.[33–39] Since the influence of a carbon additive and a binder can be eliminated, this method is useful to examine the intrinsic electrochemical performance of an active material itself. However, the applicability of conventional single particle measurements is limited in terms of the size and shape of active material particles, because it is necessary to use the measurement system in which a manipulator can be operated to contact a single particle with a glass-sealed microelectrode under an optical microscope. We have proposed to address these previous disadvantages in a conventional single particle measurement

*Electrochemical Society Member.
[z]E-mail: inada@ee.tut.ac.jp

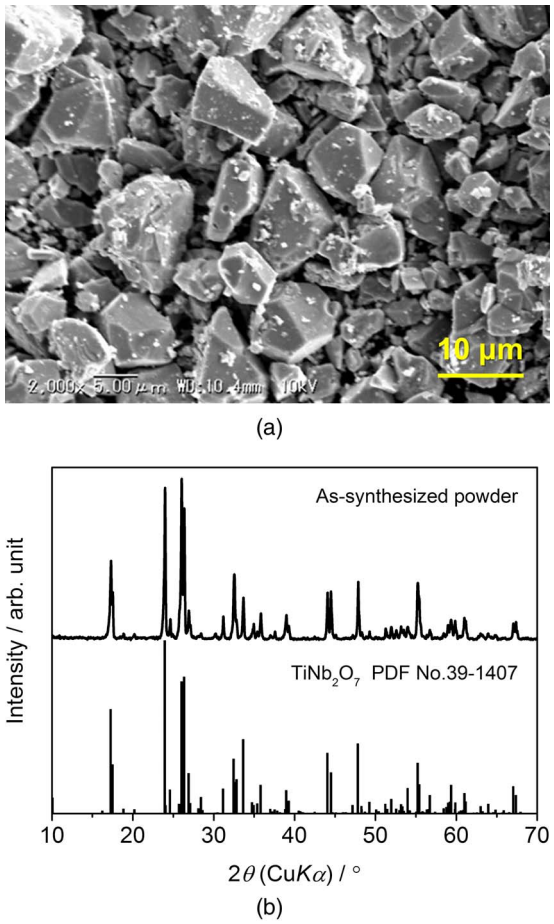

Figure 1. (a) SEM image and (b) XRD pattern for TNO powder sample annealed at 1300°C and 24 h.

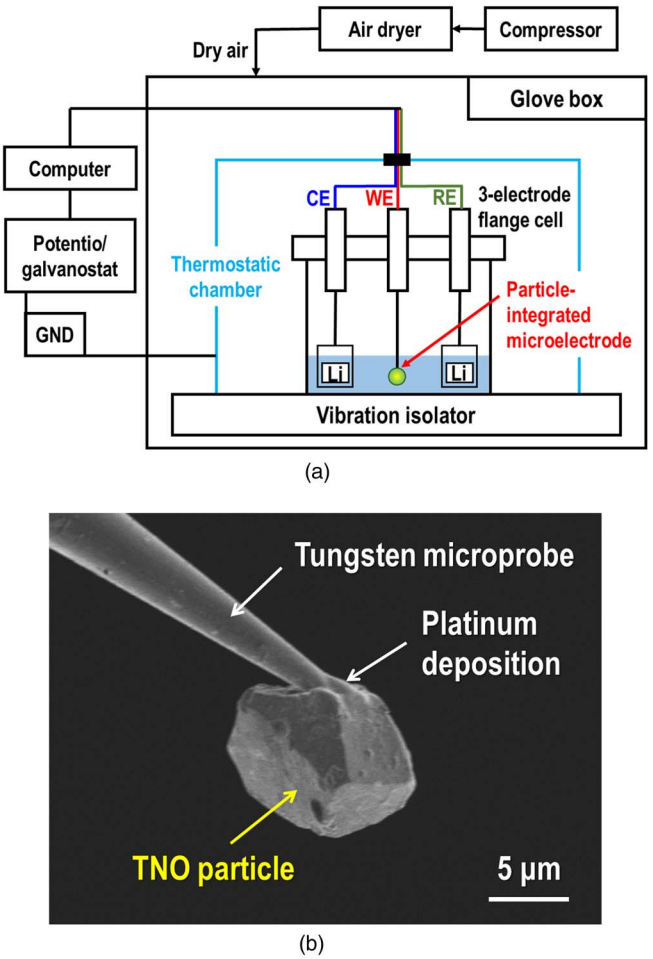

Figure 2. (a) Experimental set-up for electrochemical measurement for a single particle of an active material and (b) SEM image for TNO single particle bonded to the tip of tungsten microelectrode by platinum deposition.

by using a "particle-current collector integrated microelectrode", in which a single particle is directly bonded on a needle microelectrode (a current collector) by platinum deposition on the interface between the microelectrode and the single particle. This method makes electrical contact between a particle and a probe more stable and reliable. Using a particle-integrated microelectrode as a working electrode in a three-electrode flange cell, we successfully examined intrinsic electrochemical performance for a single particle of commercial LTO.[40,41]

In this paper, we investigated the intrinsic electrochemical performance for a $TiNb_2O_7$ (TNO) single particle with the size of 10 μm using a particle-current collector integrated microelectrode at room temperature, including the rate performance and cycling stability and for charge and discharge reaction.

Experimental

TNO powder was synthesized by a conventional solid state reaction method. Stoichiometric amounts of anatase TiO_2 (Kojundo Chemical Laboratory Co., Ltd., 99%) and Nb_2O_5 (Kojundo Chemical Laboratory Co., Ltd., 99.9%) were ground and mixed in ethanol by planetary ballmilling (Nagao System, Planet M2-3F) with zirconia balls (5 mm in diameter) for 1 hour in a zirconia pot. The mixture was dried at 90°C for 12 hours and then annealed at 1300°C for 24 hours in air using an alumina crucible, to obtain the TNO particle with a suitable size for fabricating the particle-current collector integrated microelectrode. The size and morphology for TNO powder were evaluated by a scanning electron microscopy (SEM, VE-8800, KEYENCE). Crystal phase for TNO powder was evaluated by X-ray diffractometer (MultiFlex, Rigaku) using CuKα radiation ($\lambda = 0.15418$ nm), with measurement angle range $2\theta = 5-90^\circ$ and step interval of 0.02°. As shown in Figure 1, TNO powder with the size of 5−10 μm and monoclinic shear structure was obtained and the formation of other impurity phases were not observed. Large TNO grains are formed via sintering at high temperature so that TNO powder used in this work has polycrystalline structure.

Obtained TNO powder was sonicated in ethanol for a few minutes and the solution was dropped onto an aluminum substrate followed by drying at 40°C. A needle tungsten microelectrode (PT-0001.02.01, Omniprobe) with a tip diameter < 0.5 μm was used in this work. In order to minimize the background current due to the side reaction of tungsten and/or tungsten oxides, the fluorine-coated microelectrode was prepared by dipping the tungsten microelectrode in a perfluoro amorphous polymer solution (Cytop CTL-107MK, Asahi Glass Company) and drying at 200°C for 10 minutes. After alternately dipped and dried 10 times, the finally dipped microelectrode was dried at 200°C for 1 hour.

For fabricating a particle-current collector integrated microelectrode, the fluorine-coated microelectrode and the TNO particles on the aluminum substrate were set onto a manipulator and a sample stage in a focused ion beam (FIB) apparatus (Quanta 3D, FEI Company). After attaching tungsten probe coated with the fluorinated resin to a manipulator in the FIB, the tip of the probe was cut off to expose the inner conducting part. An ionic beam with platinum was positioned and deposited on contact between the top of the cut probe and a single TNO particle under the observation by SEM and scanning ion microscope (SIM) in the FIB unit. Flange-type three-electrode cell was composed as shown in Figure 2a. TNO particle integrated with a microprobe (Figure 2b) is used as a working electrode, whereas

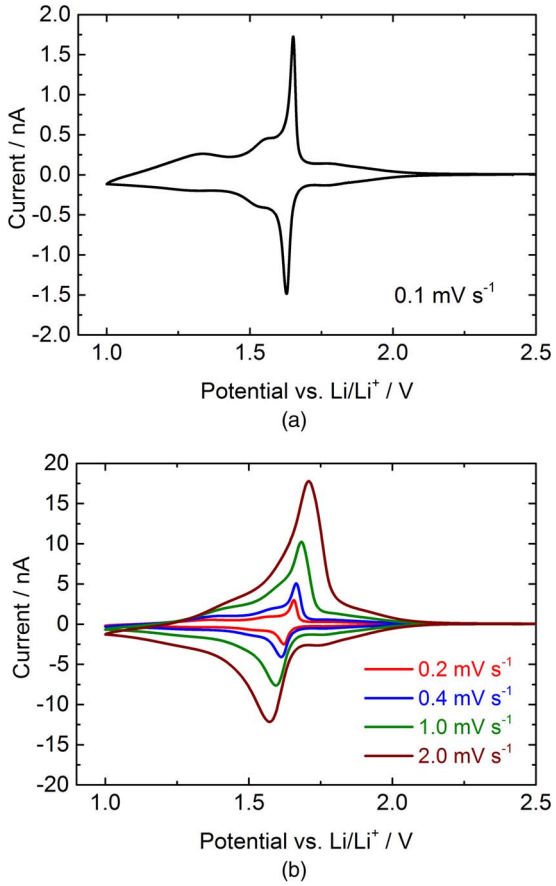

Figure 3. (a) CV curve for at scan rate of 0.1 mV s^{-1} and (b) the curves for different scan rate for TNO single particle.

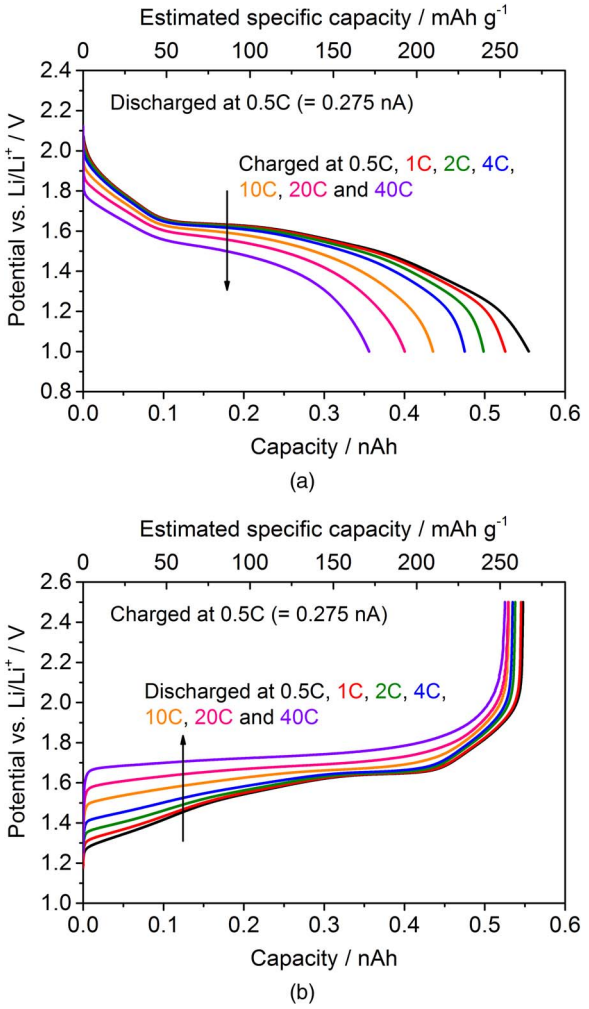

Figure 4. C-rate performance for TNO single particle at (a) charging (Li^+ insertion) and (b) discharging (Li^+ extraction) reactions. Discharging (charging) current was fixed to 0.5C for rate performance of charge (discharge) capacities. Estimated specific capacity (mAh g^{-1}) is shown in upper horizontal axis in each graph.

two lithium foils (5 mm × 5 mm × 0.15 mm) serve as both a counter and a reference electrodes. The electrolyte solution was 1 M $LiN(SO_2CF_3)_2$ in ethylene carbonate (EC) and propylene carbonate (PC) with a volume ratio of 1:1 (Kishida Chemical Co., Ltd.). The assembly of the cell was carried out in a glove box (DGB-100, AS ONE) filled by dry air. The fabricated three electrode cell was set in thermostatic chamber (TB-1, BAS) in a glove box filled by dry air. In order to suppress the measurement noise, both three-electrode cell and thermostatic chamber was put onto the vibration insulator (AVT-0405, Meiriz Seiki).

In order to examine the intrinsic electrochemical properties of a single TNO particle during the charge (defined as Li^+ insertion reaction) and discharge (defined as Li^+ extraction reaction), cyclic voltammogram (CV), galvanostatic charge/discharge testing and galvanostatic intermittent titration testing (GITT) at temperature of 20°C were measured using potentio-galvanostat system (VSP-300, BioLogic) with a highly sensitive electrometer. For the CV measurements, the cell was cycled at scan rate from 0.1−2 mV s^{-1} and the potential range from 1.0 to 2.5 V vs. Li/Li^+. Based on the CV data at 0.1 mV s^{-1}, the current corresponding to 1C rate for a TNO single particle was calculated to be 0.55 nA. Galvanostatic charge and discharge curves was measured at various current rate condition and potential range from 1.0 to 2.5 V vs. Li/Li^+. GITT testing was carried out in both charge and discharge reaction process by repeating application of pulse current with the amplitude of 2.75 nA (= 5C) for 20 seconds followed by the rest period for 900 seconds in a potential range from 1.0 to 2.5 V vs. Li/Li^+.

Results and Discussion

Figure 3a shows the CV curve for a TNO single particle measured at a scan rate of 0.1 mV s^{-1}. The profile of redox current in TNO single particle is similar with that for TNO composite electrode reported in the literatures.[23,24] Sharp main current peaks in both anodic and cathodic reactions are clearly detected at 1.65−1.66 V, while the pairs for small current peaks are also confirmed at 1.80 V and 1.55 V. Another broad peak for cathodic current is detected at lower potential around 1.3 V, while corresponding anodic current peak is not visible clearly, indicating that the reaction kinetics in Li^+ insertion and extraction processes are different at the potential below 1.5 V. The change in CV curves for TNO single particle with increasing the scan rate from 0.2 to 2.0 mV s^{-1} is shown in Figure 3b. As can be seen, the magnitude of both cathodic and anodic currents increase and the polarization becomes larger as the scan rate increases, and the separation of redox current peaks becomes difficult at higher scan rate. In addition, the magnitude for cathodic current is larger than anodic one at fixed scan rate, suggesting that the Li^+ extraction reaction in a TNO particle is faster than Li^+ insertion reaction.

Figures 4a and 4b show charging (Li^+ insertion) and discharging (Li^+ extraction) curves at different C-rate from 0.5C to 40C for TNO single particle. It is worth to note that for measuring C-rate dependence of charging (or discharging) curves, the discharging (or charging) current rate was fixed to 0.5C. At 0.5C, reversible capacity of TNO particle is estimated to be 0.55 nAh and the discharge (Li^+ extraction) reaction start at the potential of 1.18 V vs. Li/Li^+. From the quasi open-circuit voltage (OCV) curves measured in TNO composite electrodes

examined in the literatures,[23,24] the specific capacity for TNO above 1.18 V vs. Li/Li$^+$ is approximately 265 mAh g^{-1}. By addressing this fact, we consider that the capacity of 0.55 nAh in TNO particle used in this work corresponds to 265 mAh g^{-1} and 3.4 Li$^+$ are inserted and extracted reversibly in TNO particle at 0.5C. Both the charge and discharge capacities are decreased monotonically with increasing C-rate, but the capacity retention in discharging process is much higher than in charging process, which is similar with LTO.[12,13,40,41] At fixed current rate of 40C, the discharge capacity attains to 0.52 nAh (= 250 mAh g^{-1}) but the charge capacity is only 0.36 nAh (= 173 mAh g^{-1}). This is consistent with the expectation derived from CV curves at different scan rates as shown in Figure 3b, and indicates that the Li$^+$ extraction reaction in a TNO particle is faster than Li$^+$ insertion reaction.

In order to discuss the difference in reaction kinetics for Li$^+$ insertion and extraction processes in TNO single particle, GITT curves measured in both charging and discharging reactions are shown in Figures 4a and 4b. In the measurements, we repeated the application for pulse current with the magnitude of 2.75 A for 20 seconds followed by the rest period for 900 seconds at the potential from 1 to 2.5 V vs. Li/Li$^+$. Open circuit voltages can be estimated as equilibrium voltages at each step for applying a pulse current. Large overvoltages for electrochemical reaction in a TNO particle are confirmed at equilibrium potential below 1.4 V and the overvoltages increases with increasing Li$^+$ contents in TNO. As reported in the literatures for TNO composite electrodes,[19,23] the distortion of local structure and repulsive interaction from adjacent Li$^+$ ions in TNO become significant at equilibrium potential below 1.4 V (corresponding to $x > 3$ in lithiated TNO, $Li_xTiNb_2O_7$). It is also evident that the magnitude of overvoltage at the potential below 1.4 V for Li$^+$ insertion reaction is significantly larger than that for Li$^+$ extraction reaction, while the equilibrium potential above 1.6 V, the overvoltages in charge and discharge reactions are nearly the same level.

From the data for GITT analysis shown in Figure 5, we tried to estimate apparent chemical diffusion coefficient $D_{Li}{}^+$ in a TNO single particle, by assuming that the particle has a spherical shape with the radius of 5 μm. Apparent $D_{Li}{}^+$ is generally calculated as following Equation 1 derived from Fick's second law:[23,42]

$$D_{Li^+} = \frac{4}{\pi\tau}\left(\frac{N_m V_m}{S}\right)^2\left(\frac{\Delta E_s}{\Delta E_t}\right)^2 \quad (\tau \ll L^2/D_{Li^+}) \qquad [1]$$

Here, τ is the time during which constant pulse current is applied, S is the total contact area between an electrolyte and an electrode, N_m is the molar number and V_m is molar volume of active material, respectively. ΔE_s is the change of the equilibrium potential during a single-step GITT experiment, and ΔE_t is the total change of the electrode potential eliminating the *IR*-drop during a constant pulse current. In our assumption mentioned above, S is calculated by a surface area for a sphere with the radius of 5 μm. The *IR*-drop was determined by monitoring the relationship between square root of τ and the potential in a single-step of GITT experiment.[23] As shown in Figure 6, calculated $D_{Li}{}^+$ values in TNO single particle is relatively larger than other lithium inserted oxide materials such as LTO.[11,12] The assumed surface area for the calculation may be smaller than the active surface area of TNO particle, which would result into the overestimation of $D_{Li}{}^+$. In addition, the rest period after applying current pulse also influences on ΔE_s and consequently, it is considered that calculated $D_{Li}{}^+$ values shown in Figure 6 may be slightly overestimated. It is also evident that $D_{Li}{}^+$ in TNO single particle varies depending on the equilibrium potential. At the potential above 1.7 V, apparent $D_{Li}{}^+$ in both Li$^+$ insertion and extraction processes is nearly the constant and as high as 10^{-9} cm^2 s^{-1}. On the other hand, $D_{Li}{}^+$ decreases to 10^{-10} cm^2 s^{-1} at the potential around 1.65 V, which is considered to be caused by transfer from homogeneous solid-solution phase reaction to two-phase coexistence one in TNO.[19,23] It is evident that $D_{Li}{}^+$ increases at the potential of 1.60 V due to the transition to solid-solution phase reaction, and then decreases monotonically with decreasing the potential below 1.5 V. At the potential below 1.60 V, $D_{Li}{}^+$ in Li$^+$ insertion process is lower than in Li$^+$ extraction process and the deviation becomes remarkable below 1.35 V. Although the detailed mechanism for the difference in $D_{Li}{}^+$ in charge and discharge process in TNO single particle is not fully clarified at present stage, this is one of the main factors to cause the difference in rate performance in charge and discharge reaction observed in Figures 2 and 3.

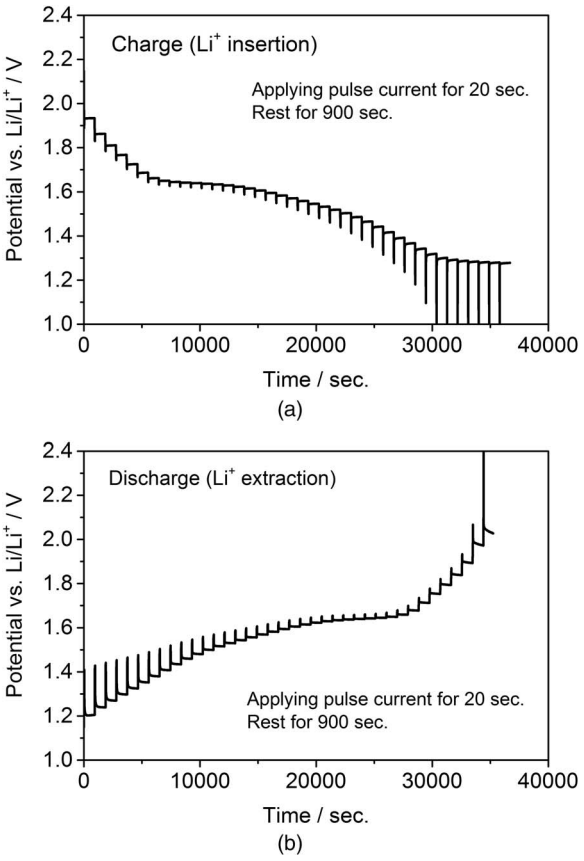

Figure 5. GITT curves for TNO single particle at (a) charging process and (b) discharging process.

Finally, cycling stability for charge and discharge reaction of TNO particle at various condition were shown in Figure 7: (a) current rates were changed from 1C to 100C every 5 cycles, (b) current rate was fixed to 10C for 2000 cycles and (c) current was fixed to 1C for 125 cycles. In the right vertical axis of each graph, estimated

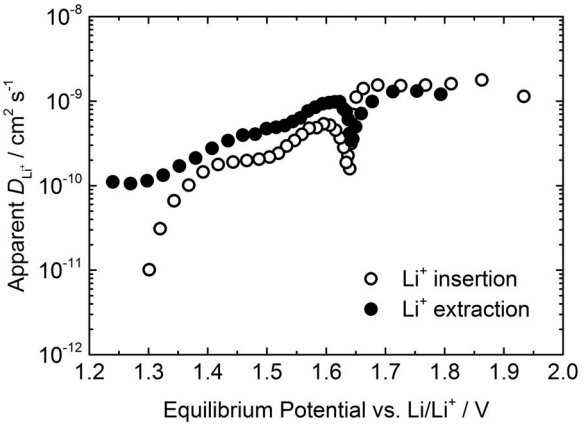

Figure 6. Apparent Li$^+$ diffusion coefficient for TNO single particle for Li$^+$ insertion and extraction process plotted against the equilibrium electrical potential vs Li/Li$^+$.

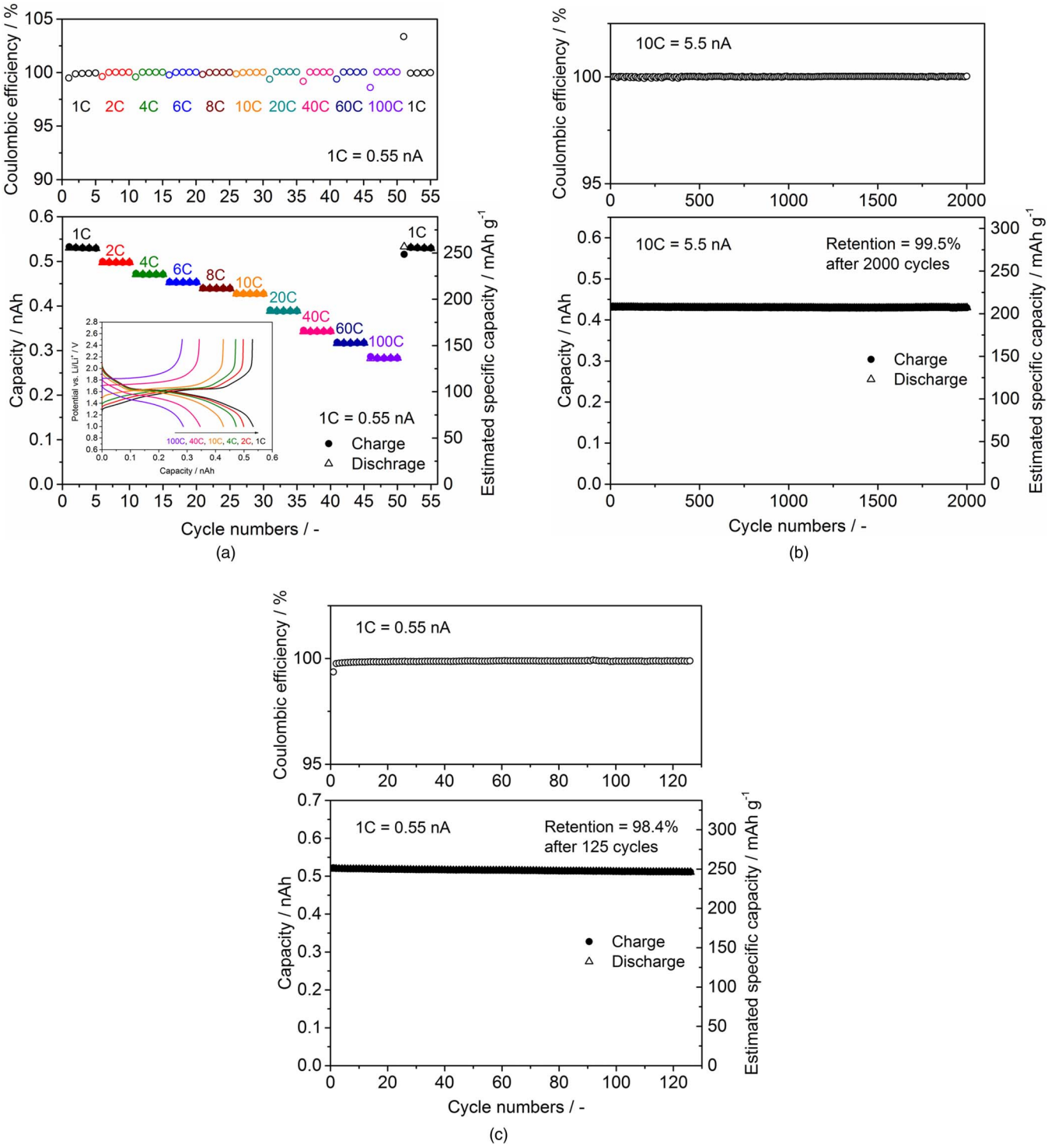

Figure 7. (a) Charge and discharge capacities and coulombic efficiency for TNO single particle at different fixed current from 0.5C to 100C. Inset in (a) is galvanostatic charge and discharge curves at each current. Cycling stability for TNO single particle at different C-rate, 10C for 2000 cycles and 1C for 125 cycles are also shown in (b) and (c). Note that the data in (b) are picked up every 10 cycles.

specific capacity of TNO particle is plotted. It is worth to note that the measurements were carried out in series from (a) to (c). During whole measurement, coulombic efficiency for charge and discharge reactions in TNO particle is nearly 100%, indicating the stability and reliability of the single particle measurements in this study. As shown in Figure 7a, charge and discharge capacities were in good agreement at each current rate and capacity fading with cycling was not confirmed. After the measurement at 100C, we measured the testing at 1C again but TNO particle maintain the initial capacity. As shown in Figure 7b, TNO particle shows outstanding cycling stability at current rate 10C. The capacity retention after 2000 cycles was estimated to be 99.5%. Reversible capacity of 0.43 nAh at 10C is corresponding to specific capacity of 209 mAh g^{-1}, so that 2.7 Li^+ are inserted and extracted reversibly without no degradation during the cycling. Then, we measured galvanostatic testing at 1C and TNO particle and confirmed good cycling stability. Although the capacity fading at 1C

was slightly faster than at 10C, the retention at 1C was 98.4% after 125 cycles. The reversible capacity at 1C is confirmed at 0.51−0.52 nAh, which corresponds to 246−252 mAh g^{-1} and approximately 3.2 Li^+ are inserted and extracted reversibly. It is considered that higher utilization for electrochemical reaction in TNO particle causes larger structural and volume changes and accelerates the capacity fading slightly. However, these results indicate excellent intrinsic cycling stability for charge and discharge reaction of TNO.

Conclusions

The electrochemical properties of $TiNb_2O_7$ (TNO) single particle was characterized using a particle-current collector integrated microelectrode. Cyclic voltammogram and C-rate dependence of charge and discharge capacities indicate faster reaction during Li^+ extraction (i.e. discharge) than Li^+ insertion (i.e. charge) of TNO particle. GITT analysis shows that at the equilibrium potential below 1.5 V, apparent chemical diffusion coefficient of Li^+ in TNO at Li^+ extraction process is much larger than at Li^+ insertion one at the equilibrium potential below 1.5 V vs. Li/Li^+, which may influence on the difference in rate performance in charge and discharge reaction for TNO. Moreover, charge and discharge reactions for TNO single particle were stably cycled for 2000 cycles at 10C, indicating excellent intrinsic stability of TNO for Li^+ insertion and extraction reactions.

Acknowledgments

This work was partly supported by Research Grants from The Hibi Science Foundation and JSPS KAKENHI grant Numbers 15H03963 and 18H01427 from Japan Society for the Promotion of Science (JSPS). Fabrication of particle – current collector integrated microelectrode was done using a Quanta 3D (FEI Company) FIB apparatus in the Cooperative Research Facility Center at Toyohashi University of Technology.

ORCID

Ryoji Inada https://orcid.org/0000-0002-6357-092X
Tomohiro Tojo https://orcid.org/0000-0001-9712-5974

References

1. J. M. Tarascon and M. Armand, *Nature*, **414**, 359 (2001).
2. B. Scrosati and J. Garche, *J. Power Sources*, **195**, 2419 (2010).
3. J. B. Goodenough and Y. Kim, *J. Power Sources*, **196**, 6688 (2011).
4. Z. Chen, I. Belharouak, Y.-K. Sun, and K. Amine, *Adv. Funct. Mater.*, **23** 959 (2013).
5. T. Ohzuku, A. Ueda, and N. Yamamoto, *J. Electrochem. Soc.*, **142**, 1431 (1995).
6. D. Yoshikawa, Y. Kadoma, J. M. Kim, K. Ui, N. Kumagai, N. Kitamura, and Y. Idemoto, *Electrochim. Acta*, **55**, 1872 (2010).
7. M-S. Song, A. Benayad, Y-M. Choi, and K-S. Park, *Chem. Commun.*, **48**, 516 (2011).
8. Z. Yu, X. Zhang, G. Yang, J. Liu, J. Wang, R. Wang, and J. Zhang, *Electrochim. Acta*, **56**, 8611 (2011).
9. Q. Zhang, C. Zhang, B. Li, D. Jiang, S. Kang, X. Li, and Y. Wang, *Electrochim. Acta*, **107**, 139 (2013).
10. H. Song, T. G. Jeong, Y. H. Moon, H. H. Chun, K. Y. Chung, H. S. Kim, B. W. Cho, and Y. T. Kim, *Sci. Rep.*, **4**, 4350 (2014).
11. N. Takami, H. Inagaki, T. Kishi, Y. Harada, Y. Fujita, and K. Hoshina, *J. Electrochem. Soc.*, **156**, A128 (2008).
12. N. Takami, K. Hoshina, and H. Inagaki, *J. Electrochem. Soc.*, **158**, A725 (2011).
13. R. J. Cava, D. W. Murphy, and S. M. Zahurak, *J. Electrochem. Soc.*, **130**, 2345 (1983).
14. J. T. Han, Y. H. Huang, and J. B. Goodenough, "New anode framework for rechargeable lithium batteries", *Chem. Mater.*, **23**, 2027 (2011).
15. J. T. Han and J. B. Goodenough, *Chem. Mater.*, **23**, 3404 (2011).
16. X. Lu, Z. Jian, Z. Fang, L. Gu, Y. S. Hu, W. Chen, Z. Wanga, and L. Chen, *Energy Environ. Sci.*, **4**, 2638 (2011).
17. K. Tang, X. K. Mu, P. A. Aken, Y. Yu, and J. Maier, *Adv. Energy Mater.*, **3**, 49 (2012).
18. S. Jayaraman, V. Aravindan, P. S. Kumar, W. C. Ling, S. Ramakrishna, and S. Madhavi, *ACS Appl. Mater., Interfaces*, **6**, 8660 (2014).
19. B. Guo, X. Yu, X. G. Sun, M. Chi, Z. A. Qiao, J. Liu, Y. S. Hu, X. Q. Yang, J. B. Goodenough, and S. Dai, *Energy & Environ. Sci.*, **7**, 2220 (2014).
20. C. Yang, C. Lin, S. Lin, Y. Chen, and J. Li, *J. Power Sources*, **328**, 336 (2016).
21. C. Lin, S. Yu, S. Wu, S. Lin, Z-Z. Zhu, J. Lia, and L. Lu, *J. Mater. Chem. A*, **3**, 8627 (2015).
22. H. Song and Y-T. Kim, *Chem. Commun.*, **51**, 9849 (2015).
23. K. Ise, S. Morimoto, Y. Harada, and N. Takami, *Solid State Ionics*, **320**, 7 (2018).
24. N. Takami, K. Ise, Y. Harada, T. Iwasaki, T. Kishi, and K. Hoshina, *J. Power Sources*, **396**, 218 (2018).
25. R. Inada, T. Mori, R. Kumasaka, R. Ito, T. Tojo, and Y. Sakurai, *Int. J. Appl. Ceram. Technol.*, **16**, 264 (2019).
26. X. Wu, J. Myao, W. Han, Y. S. Yu, D. Chen, J. S. Lee, J. Kim, and L. Chen, *Electrochem. Commun.*, **25**, 39 (2012).
27. C. Yang, S. Yu, Y. Ma, C. Lin, Z. Xu, H. Zhao, S. Wu, P. Zheng, Z-Z Zhu, J. Li, and N. Wang, *J. Power Sources*, **360**, 470 (2017).
28. T. Takashima, T. Tojo, R. Inada, and Y. Sakurai, *J. Power Sources*, **276**, 113 (2015).
29. C. F. Lin, S. Yu, H. Zhao, S. Q. Wu, G. Z. Wang, L. Yu, Y. F. Li, Z. Z. Zhu, J. B. Li, and S. W. Lin, *Sci. Rep.*, **5**, 17836 (2015).
30. S. Deng, Z. Luo, Y. Liu, X. Lou, C. Lin, C. Yang, H. Zhao, P. Zheng, Z. Sun, J. Li, N. Wang, and H. Wu, *J. Power Sources*, **362**, 250 (2017).
31. C. Yang, S. Deng, C. Lin, S. Lin, Y. Chen, J. Li, and H. Wu, *Nanoscale*, **8**, 18792 (2016).
32. H. Yu, X. Cheng, H. Zhu, R. Zheng, T. Liu, J. Zhang, M. Shui, Y. Xie, and J. Shu, *Nano Energy*, **54**, 227 (2018).
33. K. Dokko, N. Nakata, and K. Kanamura, *J. Power Sources*, **189**, 783 (2009).
34. H. Munakata, B. Takemura, T. Saito, and K. Kanamura, *J. Power Sources*, **217**, 444 (2012).
35. K. Nishikawa, H. Munakata, and K. Kanamura, *J. Power Sources*, **243**, 630 (2013).
36. J. E. Chae, K. Annaka, K. Hong, S-I. Lee, H. Munakata, S-S. Kim, and K. Kanamura, *Electrochim. Acta*, **130**, 60 (2014).
37. K. Kanamura, Y. Yamada, K. Annaka, N. Nakata, and H. Munakata, *Electrochemistry*, **84**, 759 (2016).
38. K. Nishikawa, N. Zettsu, K. Teshima, and K. Kanamura, *Electrochemistry*, **85**, 72 (2017).
39. K. Nishikawa, N. Zettsu, K. Teshima, and K. Kanamura, *J. Electroanal. Chem.*, **799**, 468 (2018).
40. Y. Sakurai, S. Kawashiri, M. Utagawa, T. Tsuda, T. Tojo, and R. Inada, *ECS Meeting Abst*. **MA2015-02**, 496 (2015).
41. T. Tojo, S. Kawashiri, T. Tsuda, M. Kadowaki, R. Inada, and Y. Sakurai, *J. Electroanalytical Chem.*, submitted.
42. W. Weppner and R. Higgins, *J. Electrochem. Soc.*, **124**, 1569 (1977).